



HAL
open science

Differential cell fates of muscle stem cells are accompanied by symmetric segregation of canonical H3 histones in vivo

Brendan Evano, Gilles Le Carrou, Geneviève Almouzni, Shahrugim Tajbakhsh

► **To cite this version:**

Brendan Evano, Gilles Le Carrou, Geneviève Almouzni, Shahrugim Tajbakhsh. Differential cell fates of muscle stem cells are accompanied by symmetric segregation of canonical H3 histones in vivo. 2017. hal-03052823

HAL Id: hal-03052823

<https://hal.science/hal-03052823>

Preprint submitted on 10 Dec 2020

HAL is a multi-disciplinary open access archive for the deposit and dissemination of scientific research documents, whether they are published or not. The documents may come from teaching and research institutions in France or abroad, or from public or private research centers.

L'archive ouverte pluridisciplinaire **HAL**, est destinée au dépôt et à la diffusion de documents scientifiques de niveau recherche, publiés ou non, émanant des établissements d'enseignement et de recherche français ou étrangers, des laboratoires publics ou privés.



Distributed under a Creative Commons Attribution - NonCommercial - NoDerivatives 4.0 International License

12 **Abstract**

13 Stem cells are maintained through symmetric or asymmetric cell divisions. While various
14 mechanisms initiate asymmetric cell fates during mitosis, possible epigenetic control of this
15 process has emerged recently. The asymmetrical distribution of a canonical histone H3
16 variant during mitosis in fly germline has suggested a role for partitioning old and new
17 nucleosomes in asymmetric cell fates. Here, we provide resources for single cell assays and
18 show the asymmetric segregation of transcription factors along with old and new DNA in
19 mouse muscle stem cells *ex vivo* and *in vivo*. However, these differential fate outcomes
20 contrast with a symmetric distribution of the canonical H3.1 vertebrate variant. These
21 findings point to different evolutionary mechanisms operating in fly germline stem cells and
22 vertebrate somatic stem cells to mitigate epigenetic regulation of asymmetric cell fates.

23 A long-standing question in multicellular organisms is how epigenetic information is
24 transmitted or changed through cell division. The nucleosome is the basic unit of chromatin
25 and notably contributes to gene expression regulation through its composition (histone
26 variants and modifications). It is therefore particularly critical to determine how, and where in
27 the genome, the choice of histone variants, their turnover and post-translational modifications
28 contribute to the maintenance or switch of a particular cell fate.

29 Histone dynamics has been addressed with a variety of approaches, on bulk chromatin
30 or at specific loci. Stable isotope labeling followed by mass spectrometry analysis notably
31 revealed differences in turnover rates of the histone H3 variants H3.1 and H3.3¹. Fluorescent
32 tags were used to assess global incorporation or inheritance patterns of H3 variants in *D.*
33 *melanogaster*^{2,3}. Additionally, photo-bleaching, photo-activation and photo-conversion have
34 been used to measure histone dynamics on short timescales⁴. Complementary approaches
35 were developed to measure locus-specific histone dynamics, by sequential expression of
36 tagged histones followed by chromatin immunoprecipitation and DNA sequencing^{5,6}, which
37 have poor temporal resolution, or by metabolic labeling of histone proteins, which has a better
38 resolution but does not distinguish between different histone variants⁷. Although these
39 methods provided significant insights into chromatin dynamics, they suffer from specific
40 downsides, from lack of positional information to delays in expression of inducible reporters.
41 In addition, current knowledge about histone dynamics arises predominantly from *in vitro*
42 models where cell fate cannot be manipulated.

43 Histone H3 variants have a major role in epigenetic maintenance during development
44 and disease^{8,9}, but tools to measure histone dynamics *in vivo* either globally or at specific loci
45 are lacking. Here, we sought to investigate histone H3 variants dynamics *in vivo* in mouse,
46 using SNAP tags as reporters and skeletal muscle stem cells as a model of changes in cell
47 fates. SNAP tags react specifically and irreversibly with benzylguanine derivatives¹⁰. A

48 number of cell-permeable SNAP substrates are available (fluorescent, biotinylated or
49 amenable to custom-probe synthesis through benzylguanine building blocks), with low
50 toxicity and allowing fast and quantitative labeling¹¹. SNAP tags were reported to work
51 efficiently and specifically *in vivo* in mice¹², and proved to be superior to classical fluorescent
52 proteins in terms of spectral flexibility, signal-to-noise fluorescence and resistance to
53 histological sample preparations^{12,13}. Further, SNAP tags allow the development of
54 functionalities *via* synthetic substrates that cannot be achieved with classical genetically
55 encoded reporters¹⁴. Finally, SNAP tags have been used extensively to measure histone H3
56 variants dynamics on bulk chromatin¹⁵⁻¹⁸, and were adapted recently to measure specific
57 histone variants turnover genome-wide¹⁹.

58 In most tissues, stem cells self-renew and give rise to daughter cells committed to
59 differentiation, thereby ensuring both tissue homeostasis and maintenance of the stem cell
60 pool²⁰. This can be achieved through different modes of cell division, either symmetric
61 (Symmetric Cell Division, SCD), self-renewing or differentiating, or asymmetric
62 (Asymmetric Cell Division, ACD) divisions. Fine-tuning the balance between these different
63 modes is critical for proper tissue development, homeostasis and regeneration, and to prevent
64 tumorigenesis²⁰.

65 A variety of subcellular constituents, including transcripts, organelles, centrosomes or
66 sister chromatids can distribute asymmetrically between daughter cells during cell division²¹.
67 A major challenge is to understand how their biased segregation dictates asymmetric cell
68 fates²². The hypothesis of a role for replication-coupled nucleosome assembly in determining
69 asymmetric cell fates in *C. elegans* nervous system has raised much interest²³. Furthermore,
70 recent studies reported non-equivalent inheritance of specific histone variants during ACD of
71 *D. melanogaster* male germline stem cells (GSCs)^{3,24}. These findings along with the
72 importance of chromatin in cell plasticity⁹ raised the possibility of an epigenetic mechanism

73 for maintaining the identity of self-renewed stem cells while resetting the identity of their
74 differentiating sibling cells.

75 Here we sought to investigate whether the non-equivalent inheritance of specific
76 histone variants is conserved in mammals, using mouse skeletal muscle stem cells as a model.
77 Adult skeletal muscle satellite (stem) cells are mostly quiescent during homeostasis.
78 Following muscle damage, they proliferate and differentiate into muscle fibres by cell-cell
79 fusion^{25,26}. A fraction of the population self-renews and reconstitutes a *de novo* satellite cell
80 pool. This is accompanied by a temporal expression of cell fate markers, such as the
81 transcription factors Pax7 (stem), Myod (commitment) and Myogenin (differentiation).
82 Satellite cells can divide symmetrically and asymmetrically during muscle regeneration²⁷⁻²⁹,
83 which is critical for proper muscle regeneration and maintenance of the satellite cell
84 pool^{27,30,31}.

85

86 **Results**

87 To address whether the mechanism uncovered in *Drosophila* GSCs operates in a
88 somatic mammalian stem cell, we developed a pulse-chase approach to follow histone
89 variants using SNAP tags. SNAP-tagged histones have been used for addressing human H3.1
90 and H3.3 turnover during DNA replication and repair¹⁶⁻¹⁸. The asymmetric inheritance of H3,
91 but not H3.3, reported in *D. melanogaster* GSCs³ prompted us to generate mouse reporter
92 lines expressing SNAP-tagged H3.1 and H3.3 to follow their inheritance patterns during ACD
93 of satellite cells.

94 *H3.1-SNAP* and *H3.3-SNAP* transgenes were expressed in several tissues
95 (Supplementary Fig. 1a), at low levels (< 20%) compared to endogenous histone expression
96 (Supplementary Fig. 1b). SNAP labeling of embryonic fibroblasts derived from reporter mice
97 showed ubiquitous *H3.1-SNAP* expression, whereas *H3.3-SNAP* expression was lower and

98 variegated (data not shown). Furthermore, as reported¹⁶ we find that newly deposited H3.1-
99 SNAP histones overlapped with sites of DNA replication, while newly deposited H3.3-SNAP
100 histones were uncoupled from DNA replication (Supplementary Fig. 1c). These results
101 indicate that the *Tg:H3.1-SNAP* and *Tg:H3.3-SNAP* lines are faithful reporters of H3.1 and
102 H3.3 turnover in mouse primary cells.

103 To examine the distribution of parental H3.1 histones in satellite cells, adult *Tibialis*
104 *anterior* (TA) muscles were injured to induce satellite cell activation and muscle regeneration.
105 Parental H3.1 histones were SNAP-labeled prior to satellite cell isolation (labeling efficiency
106 $\approx 80\%$, Fig. 1a and Supplementary Fig. 1d). Satellite cells were isolated from compound
107 transgenic *Tg:Pax7-nGFP*³² and *Tg:H3.1-SNAP* mice by fluorescence-activated cell sorting
108 (FACS) where GFP intensity can be used to fractionate subpopulations with distinct
109 properties, such as Pax7-nGFP^{Hi} cells previously reported to divide asymmetrically 5 days
110 post-injury (dpi)²⁸. *In vivo* activated/SNAP-labeled Pax7-nGFP^{Hi} cells were isolated by FACS
111 and the ongoing cell division was monitored on micropatterns (Fig. 1a). Micropatterns
112 provide a controlled microenvironment that allows confinement of single cells and their
113 progeny³³. We and others have shown that their geometry impacts on the frequency of ACD
114 of stem cells^{29,34}. If the parental histones are partitioned equally following mitosis, the
115 fluorescent SNAP signal will be inherited equally between daughter cells. However, if the
116 parental histones are inherited asymmetrically, the fluorescent SNAP signal will be detected
117 only in a subset of daughter cells (Fig. 1b).

118 Modes of cell division were scored based on absolute presence or absence of cell fate
119 markers. Their expression level and SNAP signal intensity were further measured
120 quantitatively. We observed self-renewing and differentiating (Fig. 1c left and middle) SCDs,
121 in addition to ACDs (Fig. 1c right), as reported^{28,29}. Interestingly, we observed clones
122 containing 4 cells with two self-renewed cells (Pax7⁺) and two differentiated cells (Myog⁺),

123 indicating a switch from self-renewing SCD to ACD (Supplementary Fig. 1e). Among all
124 observed clones, the SNAP signal intensity was equivalent between daughter cells,
125 irrespective of their mode of cell division (Fig. 1c). The maximal SNAP intensity difference
126 between daughter cells was less than 8% (Fig. 1c left), while transcription factors displayed
127 differences in expression up to 80% between daughter cells in case of ACD (Fig. 1c right).
128 These results indicate that parental H3.1 histones were essentially inherited symmetrically
129 during both SCD and ACD of satellite cells.

130 H3-Thr3 phosphorylation (H3T3^P) was reported to distinguish pre-existing and newly-
131 deposited H3 in prophase, and to be required for asymmetric inheritance of old *vs.* new
132 histones in *D. melanogaster* GSCs²⁴. To further address the issue of histone inheritance, we
133 investigated the distribution of H3T3^P in *in vivo* activated/SNAP-labeled Pax7-nGFP^{Hi} cells
134 on micropatterns. We readily detected H3T3^P signals in mitotic cells, colocalizing with SNAP
135 signals yet not restricted to a subset of chromatids in early mitosis (Fig. 1d). These
136 observations indicate that H3T3^P did not point to a differential distribution of old *vs.* new
137 histones in early mitosis of satellite cells.

138 Within adult muscles, satellite cells reside in a specific niche and a complex balance
139 between extrinsic and intrinsic cues is required for proper satellite cell proliferation and cell
140 fate determination³⁵. As with other stem cell niches³⁶, the composition of the satellite cell
141 microenvironment is dynamic during muscle regeneration³⁷, raising the possibility that some
142 niche factors that cannot be modelled *ex vivo* might drive ACDs. Although ACDs have been
143 reported extensively *ex vivo*, to the best of our knowledge, only one study has demonstrated
144 asymmetry involving transcription factors in a vertebrate model system *in vivo*³⁸.

145 Therefore, we established a clonal tracing strategy to examine two-cell clones in
146 regenerating muscles *in vivo* (Fig. 2a and Fig. 2b), together with SNAP-labeling of parental
147 H3.1 histones (*in vivo* labeling efficiency \approx 60%, Supplementary Fig. 2b). As previously,

148 modes of cell division were scored based on absolute presence or absence of cell fate markers.
149 Their expression level and SNAP signal intensity were further measured quantitatively. We
150 observed self-renewing (66.7%, n=98 of 147 cell pairs, Fig. 2c and Fig. 2d left) and
151 differentiating (6.8%, n=10 of 147 cell pairs, Fig. 2c and Fig. 2d middle-left) SCDs, in
152 addition to ACDs (23.1%, n=34 of 147 cell pairs, Fig. 2c and Fig. 2d middle-right and right).
153 Notably, the relative frequencies of the different modes of cell division observed *in vivo*
154 correspond to those on micropatterns *ex vivo*²⁹. Among all clones analysed, we observed an
155 equivalent SNAP signal between daughter cells (Fig. 2d). Interestingly, a difference in SNAP
156 signal intensity (up to 40%) between daughter cells was noted for a limited number ($\approx 5\%$) of
157 divisions (Fig. 2d left and right, Fig. 2g right). However, the differences in SNAP intensity
158 were lower than the observed differences in expression of cell fate markers, resulting from
159 fluctuations in expression in case of SCD (Fig. 2d left) or asymmetric fate decisions (Fig. 2d
160 right). Further, we did not detect examples showing exclusive distribution of parental histones
161 to one daughter. These results point to a symmetric inheritance of parental H3.1 histones,
162 irrespective of the mode of cell division *in vivo*.

163 Notably, differences in SNAP signals between daughter cells were not observed *ex*
164 *vivo* on micropatterns (Fig. 1c), suggesting variable H3.1 turnover rates between daughter
165 cells *in vivo* and *ex vivo*. These observations highlight the importance of addressing epigenetic
166 identity and plasticity *in vivo*. Finally, the SNAP signal was readily detected after histological
167 preparation (strong fixation and heat-induced epitope retrieval), while the mGFP fluorescence
168 was lost and required immunodetection, confirming the superiority of synthetic SNAP
169 fluorophores over classical fluorescent proteins.

170 The asymmetric segregation of stem (Pax7) and differentiation (Myogenin)
171 transcription factors was previously reported to correlate in part with non-random DNA
172 segregation (NRDS) *ex vivo*, where old DNA strands are inherited by the stem cell and new

173 DNA strands by the committed cell^{28,29}. NRDS has been hypothesized to be a consequence of
174 epigenetic mechanisms, possibly involving distribution of old and new histones or
175 nucleosome pools²²; however NRDS has not been shown robustly *in vivo* largely due to
176 technical challenges. To examine parental H3.1 histone distribution and NRDS *in vivo*, we
177 adopted the same strategy as above, together with a 5-ethynyl-2'-deoxyuridine (EdU) pulse-
178 chase labeling (Fig. 2a and Fig. 2e) to identify both old DNA strands (EdU pulse) and new
179 DNA strands (EdU chase).

180 We observed clonal examples of random DNA segregation (23.1%, n=12 of 52 cell
181 pairs, Fig. 2f and Fig. 2g left) and non-random DNA segregation (76.9%, n=40 of 52 cell
182 pairs, Fig. 2f and Fig. 2g middle and right). Interestingly, 22.5% of the cell pairs with NRDS
183 showed asymmetric Myogenin expression (n=9 of 40 NRDS cell pairs, Fig. 2f and Fig. 2g
184 right), with Myogenin being expressed in the EdU-negative daughter cell, as reported
185 previously *ex vivo* where parental DNA strands are labeled and inherited by the Pax7-
186 expressing cell^{28,29}. Among all the clones analysed, the SNAP signal was equivalent between
187 daughter cells (Fig. 2g), indicating a symmetric parental H3.1 inheritance, independent of the
188 mode of DNA segregation.

189

190 **Discussion**

191 Here we demonstrate that SNAP tags are powerful tools to investigate histone
192 dynamics in mice *in vivo*. Our results indicate that parental H3.1 histones are equally inherited
193 in the vast majority of dividing mouse satellite cells, *ex vivo* as *in vivo*, during asymmetric
194 cell fate decisions with defined stem cell and differentiated cell transcription factors, as well
195 as non-random segregation of DNA. Asymmetric histone H3 inheritance has uniquely been
196 reported in *D. melanogaster* GSCs to date and was correlated with the execution of different
197 cell fate programs following cell division^{3,24}. A two-step mechanism was proposed where old

198 and new histones are incorporated into different sister chromatids during S phase, followed by
199 differential recognition and segregation of old and new sister chromatids by the mitotic
200 apparatus^{3,24}. This requires both an asymmetric distribution of histones at the replication fork,
201 and strictly unidirectional DNA replication throughout the genome. Recently, two reports
202 highlighted that while histone partitioning in the wake of the replication fork is inherently
203 asymmetric between leading and lagging DNA strands, components of the replication
204 machinery compensate to ensure an equal distribution of parental histones between sister
205 chromatids^{39,40}. Asymmetric histone distribution in *Drosophila* GSCs might then result from
206 retention of parental histones on the leading strand and preferential unidirectional DNA
207 replication⁴¹. While our results address global inheritance of parental histones and cannot
208 exclude local limited asymmetry, notably at the replication fork, the discrepancy observed
209 between *D. melanogaster* GSCs and our analysis of mouse satellite cells might indicate that
210 the molecular mechanisms of asymmetric histone inheritance are not generally conserved
211 through evolution, or alternatively between germline and somatic stem cells.

212 Our results show unambiguously for the first time NRDS *in vivo* and indicate that this
213 process is not driven by a global asymmetric inheritance of old and new pools of H3.1.
214 Nevertheless, according to the silent sister hypothesis⁴², epigenetic differences might exist
215 between sister chromatids due to their relative difference in age. Asymmetric recognition of
216 centromeres would then be the basis for NRDS, which would in turn lead to asymmetric gene
217 expression and cell fate decisions. In this context, it is interesting to note that CENP-A, the
218 centromeric H3 variant, was shown to be inherited asymmetrically during stem cell divisions
219 in the fly midguts⁴³, a possibility to explore in the future.

220 Finally, while our study investigated inheritance of bulk histones, the tools and
221 methodologies reported here, combined with the recent advent of time-ChIP^{19,44}, will allow
222 genome-wide tracking of histone variant turnover rates. This can be done in a wide variety of

223 mouse primary cell types in their *in vivo* environment thereby facilitating investigations of
224 how epigenetic identity is maintained in stem cells, and remodeled in their differentiating
225 progeny.

226

227 **Methods**

228 Mouse strains

229 *Tg:Pax7-nGFP*³², *Pax7^{CreERT2}*⁴⁵ and *R26^{mTmG}*⁴⁶ were described previously. Breeding
230 was performed on an F1:C57BL6/DBA2 background. 6-8 weeks-old male littermates were
231 used in this study, heterozygous for each allele used. Animals were handled according to
232 national and European community guidelines, and protocols were approved by the ethics
233 committee at Institut Pasteur.

234

235 Cell lines and culture conditions

236 Primary fibroblasts were derived at E13.5 and cultured in DMEM GlutaMAX
237 (ThermoFisher) 10% Fetal Bovine Serum (FBS) 1% Penicillin-Streptomycin (PS,
238 ThermoFischer) at 37°C 5% CO₂ 3% O₂.

239 Satellite cells were plated on glass coverslips coated with Matrigel (Corning) for 30 min
240 at 37°C or on micropatterns in satellite cell medium (40% DMEM 40% MCDB (Sigma) 20%
241 FBS 2% Ultrosor (Pall) 1% PS).

242

243 Establishment of H3.1/H3.3-SNAP mouse strains

244 Mouse H3.1 (resp. H3.3) coding sequence was PCR amplified (Phusion Taq polymerase,
245 New England Biolabs) from mouse primary fibroblasts cDNA (SuperScript III Reverse
246 Transcriptase, ThermoFisher) with NotI_mH3.1_F (resp. NotI_mH3.3_F) and
247 DPPVAT_mH3.1_R (resp. DPPVAT_mH3.3_R) primers, PCR-fused to a SNAP tag
248 amplified from pSNAPm (New England Biolabs) with DPPVAT_SNAP_F and
249 BamHI_SNAP_R primers, and cloned in pGEM-T easy (Promega) with T4 DNA ligase (New
250 England Biolabs). A DPPVAT linker was included between histone coding sequences and the
251 SNAP tag as in ^{16,17}. H3.1-SNAP (resp. H3.3-SNAP) EcoRI/BamHI (New England Biolabs)
252 fragment was subcloned in a pCAG SV40 Puro plasmid between the EcoRI and BamHI sites
253 downstream the CAG promoter and upstream an SV40 early polyA termination sequence.

254 CAGG H3.1/H3.3-SNAP polyA SpeI/KpnI (New England Biolabs) DNA fragments were
255 microinjected in fertilized oocytes to derive transgenic lines.

256 Genotyping was performed by PCR from ear punch biopsies with CAG_For and
257 DPPVAT_mH3.1_R or DPPVAT_mH3.R_R primers. *H3.1-SNAP* transgene insertion was
258 mapped to chromosome 7 by inverse PCR (gDNA digestion with SacI (New England
259 Biolabs), intramolecular ligation with T4 DNA ligase, PCR amplification with SV40
260 PolyA_F and SNAP qPCR_R primers). *H3.3-SNAP* transgene insertion was mapped to
261 chromosome 10 by inverse PCR (gDNA digestion with BamHI, intramolecular ligation with
262 T4 DNA ligase, PCR amplification with SNAP qPCR_F and CAG_R3 primers). Primers used
263 are listed in Supplementary Table 1.

264

265 RT-qPCR

266 Organs were homogenized in TRIzol (ThermoFisher) and RNA extracted following
267 manufacturer's instructions. gDNA was eliminated with Ambion DNaseI (ThermoFisher)
268 and reverse transcription performed with SuperScript III Reverse Transcriptase
269 (ThermoFisher). RNA was eliminated with RNaseH endonuclease (Roche) for 20 min at
270 37°C. mRNAs level was assessed with SYBR green master mix (Roche) and analysis was
271 performed using the $2^{-\Delta Ct}$ method⁴⁷. RT-qPCR analyses have been normalized with *Tbp*.
272 Specific forward and reverse primers used for RT-qPCR are listed in Supplementary Table 1.

273

274 Western blot

275 Histones were extracted following⁴⁸ and protein concentration measured with the Pierce
276 BCA Protein Assay Kit (ThermoFisher). 1 μ g of histones was run on 4-12% Bis-Tris Gel
277 NuPAGE (ThermoFisher) in NuPAGE MES SDS Running Buffer (ThermoFisher) and
278 transferred on a nitrocellulose membrane (Hybond ECL, Sigma) in 1X Tris-Glycine-SDS
279 buffer (Euromedex) with 20% ethanol. Equivalent loading was evaluated from Ponceau
280 staining of the membrane. The membrane was then blocked with 5% non-fat milk in Tris
281 Buffer Saline (TBS) Tween 0.05% (TBS-T) for 20 min at RT and probed with specific
282 primary antibodies overnight at 4°C in TBS-T 5% milk. After three washes in TBS-T, the
283 membrane was incubated with HRP-conjugated secondary antibodies in TBS-T for 30 min at
284 RT, washed three times in TBS-T, and revealed by chemiluminescence (Pierce ECL Plus
285 Western Blotting Substrate, ThermoFisher) with autoradiography films (Hyperfilm ECL, GE
286 Healthcare).

287

288 SNAP labeling

289 *In vitro* SNAP quenching (Supplementary Fig. 1c) was performed with 10 μ M SNAP
290 Cell Block (New England Biolabs) for 30 min at 37°C, followed by three washes with culture
291 medium. *In vitro* SNAP labeling was performed with 3 μ M SNAP Cell TMR Star (New
292 England Biolabs) in culture medium for 20 min at 37°C, followed by three washes with
293 culture medium, and washed in culture medium for 30 min at 37°C. Sites of DNA replication
294 were labeled with 1 μ M EdU (ThermoFisher) for 10 min at 37°C. Soluble histones were
295 extracted with CSK buffer prior to fixation as in ¹⁶. EdU incorporation was detected with the
296 Click-iT Plus Alexa Fluor 488 Imaging Kit (ThermoFisher) as recommended.

297 *Ex vivo* SNAP labeling (Fig. 1a) was performed by incubating dissected and minced TA
298 muscles in 1 ml satellite cell medium containing 3 μ M SNAP Cell SiR 647 (New England
299 Biolabs, S9102S) for 30 min at 37°C with gentle agitation. Muscles were centrifuged at 500g
300 for 5 min, supernatant was discarded and muscles resuspended in 1 ml DMEM. Muscles were
301 centrifuged at 500g for 5 min, supernatant was discarded and muscles resuspended in
302 collagenase D/trypsin mix for satellite cell isolation (see below).

303 *In vivo* SNAP labeling was performed by injecting 10 μ l of 30 μ M SNAP Cell SiR 647
304 (New England Biolabs) in NaCl 0.9% per TA at 4 dpi under isofluorane anesthesia, 8 h before
305 tamoxifen administration (Fig. 2a). *In vivo* H3.1-SNAP labeling at 4 dpi enables specific
306 labeling of \approx 60% of satellite cells as early as 2 h post SNAP substrate injection
307 (Supplementary Fig. 2b).

308

309 Muscle injury, tamoxifen and EdU delivery

310 Muscle injury was done as described previously ⁴⁹. Briefly, mice were anesthetized with
311 0.5% Imalgene/2% Rompun. The *Tibialis anterior* (TA) muscle was injected with 15 μ l of 10
312 μ M notexin (Latoxan) in NaCl 0.9%.

313 Tamoxifen (Sigma) was reconstituted at 25 mg/ml in corn oil/ethanol (5%) and stored at
314 -20°C. Before use, tamoxifen was diluted at appropriate concentration (1 mg/ml or 0.25
315 mg/ml) with corn oil, and administered (8 μ l per g of mouse) by intragastric injection at 4
316 days post-injury and 14 h prior to sacrifice to allow for a maximum of two consecutive cell
317 divisions *in vivo* (*in vivo* satellite cells doubling time about 8 h ²⁸). We optimized conditions
318 for clonal tracing leading to two-cell clones shortly after (14 h) tamoxifen administration.
319 Clones were defined when mGFP-labeled cells were in close proximity (< 150 μ m apart,
320 Supplementary Fig. 2a and Supplementary Fig. 2c) and isolated from any other mGFP-
321 labeled cell. In addition, the definition of criteria for clonality was based on an extremely low

322 dose of tamoxifen (2 $\mu\text{g/g}$ of mouse, recombination frequency < 0.5%). We then used a
323 tamoxifen dose (8 $\mu\text{g/g}$ of mouse) inducing a recombination frequency about 10% to increase
324 the representation of the myogenic population. For each mouse, one TA muscle was used for
325 immunohistochemistry analysis, and the contralateral TA was used for determining the
326 recombination efficiency following dissociation and immunostaining.

327 EdU (ThermoFisher) was dissolved in NaCl 0.9% and injected intraperitoneally (0.3
328 $\mu\text{g/g}$ of mouse) 9 and 7 h before tamoxifen administration.

329

330 Satellite cells isolation and live-imaging

331 Dissections were done essentially as described previously⁴⁹. Injured TA muscles were
332 removed from the bone in cold DMEM, minced with scissors, and then digested with a
333 mixture of 0.08% Collagenase D (Sigma), 0.1% Trypsin (ThermoFisher), 10 $\mu\text{g/ml}$ DNase I
334 (Sigma) in DMEM for five consecutive cycles of 30 min at 37°C. For each round, the
335 supernatant was filtered through a 70 μm cell strainer (Miltenyi) and collagenase and trypsin
336 were blocked with 8% FBS on ice. Pooled supernatants from each digestion cycle were
337 centrifuged at 500g for 15 min at 4°C. The pellet was resuspended in 2 ml cold PBS
338 (ThermoFisher) and placed on top of cold Percoll layers (Sigma)(5 ml of 20% Percoll and 3
339 ml of 60% Percoll). After centrifugation at 500g for 15 min at 4°C, cells were collected from
340 the 20%-60% interphase, while dense debris were concentrated below the 60% layer. The
341 collected fraction was diluted in 40 ml DMEM 8% FBS and centrifuged at 500g for 15 min at
342 4°C. The pellet was resuspended in 500 μl satellite cell medium and filtered through a 40 μm
343 cell strainer (Falcon). Cells were plated on glass coverslips coated with Matrigel or sorted
344 (Supplementary Fig. 3) using a FACS Aria III (BD Biosciences) and collected in cold 250 μl
345 of satellite cell medium. Sorted cells were plated on micropatterns (see below) and incubated
346 at 37°C, 5% CO₂, and 3% O₂ in a Zeiss Observer.Z1 microscope connected to an LCI PlnN
347 10x/0.8 W DICII objective and Hamamatsu Orca Flash 4 camera piloted with Zen (Zeiss).
348 Cells were filmed and images were taken every 9 min with bright-field filter to ensure that
349 single cells were plated on the micropatterns and that their progeny remained confined. The
350 raw data were analysed with TrackMate⁵⁰, transformed and presented as videos.

351

352 Micropatterns

353 Micropatterns were manufactured essentially as described^{29,51}. Briefly, glass coverslips
354 (24 x 60 mm #1, Thermo Scientific Menzel) were cleaned serially in
355 H₂O/acetone/isopropanol, activated with an oxygen plasma treatment (Harrick Plasma) for 5

356 min at 30W and incubated with poly-L-lysine polyethylene glycol (PLL(20)-g[3.5]-PEG(2),
357 SuSoS) at 100 $\mu\text{g/ml}$ in 10 mM HEPES pH 7.4 at room temperature (RT) for 30 min, washed
358 twice with H₂O and stored dried at 4°C. PLL-PEG-coated slides were placed in contact with
359 an optical mask containing transparent micropatterns (Toppan Photomask) using H₂O (0.6
360 $\mu\text{l/cm}^2$) to ensure tight contact between the mask and the coverslip and then exposed to deep
361 UV light (Jelight). Micropatterned slides were subsequently incubated with 40 $\mu\text{g/ml}$
362 fibronectin (Sigma) and 5 $\mu\text{g/ml}$ fibrinogen Alexa Fluor 488 (ThermoFisher) in 100 mM
363 NaHCO₃ pH 8.3 for 25 min at RT and rinsed three times in NaHCO₃, three times in H₂O and
364 dried and transferred immediately on a 12 kPa polyacrylamide (PAA) gel on silanized glass
365 coverslips, to match the substrate rigidity of skeletal muscles⁵². 81 mm²-square glass
366 coverslips were cut out larger coverslips (22 x 22 mm #1, Thermo Scientific Menzel), cleaned
367 serially with H₂O/EtOH 70%/EtOH 100%, deep-UV-activated, silanized with 7.1% (vol/vol)
368 bind-silane (Sigma) and 7.1% (vol/vol) acetic acid in EtOH 99% for 10 min at RT, washed
369 twice with EtOH 99% and dried. Transfer of micropatterns on PAA gel was performed with 7
370 $\mu\text{l/cm}^2$ of a solution containing 7.5% acrylamide (Sigma), 0.16% bis-acrylamide (Sigma),
371 0.05% TEMED (Sigma), 0.05% APS (Sigma, A3678) in HEPES 10 mM pH 7.4 for 45 min at
372 RT. Gels were rehydrated in NaHCO₃ 100 mM pH 8.3 for 15 min at RT, detached from
373 patterned coverslips and washed with PBS three times before cell seeding.

374 Micropatterned PAA gels were transferred in an in-house-made glass-bottom 6 well Petri
375 dish to allow live-imaging and PAA embedding before immunostaining (see below). Briefly,
376 32 mm diameter glass coverslips were cleaned and silanized, a 14 x 14 x 0.45 mm piece of
377 silicone (Smooth-on) was put at the center, and coverslips were layered with a 12 kPa PAA
378 gel ('surrounding' PAA). After PAA polymerization, the coverslips were sealed (silicone) to
379 the bottom of a 6 well plate (TPP) drilled out to 30 mm diameter. The silicone at the center of
380 the PAA gel was removed and replaced with a 16 x 16 x 3 mm silicone isolator with a 10 x 10
381 x 3 mm window at the center to fit micropatterned PAA gels (9 x 9 mm) after filling with
382 PBS. The apparatus was washed several times and equilibrated with satellite cell medium.
383 Medium was removed completely and cells (250 μl) seeded within the silicone isolator on
384 micropatterns and, 90 min after plating, nonattached cells were washed with medium and
385 medium volume was adjusted to 5 ml.

386

387 Immunocytochemistry and Immunohistochemistry

388 Cells on micropatterns were fixed in 4% paraformaldehyde (PFA, Electron Microscopy
389 Sciences) in PBS containing 0.9 mM CaCl₂ and 0.5 mM MgCl₂ (PBS Ca²⁺ Mg²⁺) for 5 min at

390 RT and washed in PBS Ca^{2+} Mg^{2+} for 5 min at RT. To prevent cell loss during subsequent
391 immunostaining steps, cells were embedded in PAA. Cells were equilibrated in a solution
392 containing 3.82% acrylamide, 0.13% bis-acrylamide and 0.1% TEMED in PBS for 30 min at
393 RT, and the solution was replaced with 3.82% acrylamide, 0.13% bis-acrylamide, 0.1%
394 TEMED and 0.05% APS in PBS. The silicone isolator was carefully detached and a parafilm-
395 covered 20 x 20 mm glass coverslip (20 x 20 mm #1, Thermo Scientific Menzel) was adjusted
396 on top of the micropatterns, sitting on the ‘surrounding’ PAA. Excess polymerization solution
397 was removed and PAA allowed to polymerize for 1 h at RT. After rehydration in PBS for 15
398 min, the parafilm-covered coverslip was detached, PAA-embedded micropatterns were
399 recovered and washed several times in PBS. Cells were permeabilized in 0.5% Triton X-100
400 (Sigma) for 20 min at RT, washed three times 10 min in PBS, blocked in 10% goat serum
401 (GS, Gibco) for 4 h at RT, incubated with primary antibodies overnight at 4°C in 2% GS,
402 washed four times 1 h in PBS at 4°C, incubated with Alexa Fluor-conjugated secondary
403 antibodies and Hoechst when required overnight at 4°C in 2% GS and washed four times 1 h
404 in PBS at 4°C. For Pax7/Myod/Myog triple staining, cells were further blocked with Pax7
405 primary antibody overnight at 4°C in 2% GS, washed four times 1 h in PBS at 4°C, incubated
406 with Alexa Fluor 488-conjugated anti-Myogenin and DyLight 405-conjugated anti-Myod
407 antibodies (see below) in 2% GS overnight at 4°C and washed four times 1 h in PBS at 4°C.

408 Cells on glass coverslips were fixed in 4% PFA for 5 min at RT, washed twice in PBS,
409 permeabilized in 0.5% Triton X-100 for 5 min, blocked in 10% GS for 30 min at RT,
410 incubated with primary antibodies in 2% GS for 2 h at RT, washed in PBS three times 5 min,
411 incubated with Alexa Fluor-conjugated secondary antibodies and Hoechst for 45 min at RT,
412 washed in PBS three times 5 min and mounted in PBS Glycerol 75%.

413 For immunohistochemistry, TA muscles were fixed for 24 h in 4% PFA at 4°C, washed
414 in cold PBS four times 1 h at 4°C, equilibrated in 20 % sucrose (Sigma) overnight at 4°C,
415 embedded in Tissue Freezing Medium (Leica) and snap-frozen on liquid nitrogen. 12 μm
416 cryosections were allowed to dry at RT for 30 min and rehydrated in PBS for 15 min. Antigen
417 retrieval was performed in Tris 10 mM EDTA 1 mM pH 9 for 10 min at 95°C, followed by
418 three short PBS washes and an additional wash in PBS for 30 min at RT. Sections were
419 permeabilized in 0.5% Triton X-100 for 20 min at RT, washed three times in PBS, blocked in
420 M.O.M. Mouse Ig Blocking Reagent (Vector Laboratories) for 1 h at RT, washed three times
421 in PBS, incubated in M.O.M. Diluent (Vector Laboratories) for 5 min at RT, incubated with
422 primary antibodies (Pax7 (Fig. 2d) or 5FD (Fig. 2g), GFP, in M.O.M. Diluent) for 1 h at RT,
423 washed three times 5 min in PBS, incubated with M.O.M. Biotinylated Anti-Mouse IgG

424 Reagent (Vector Laboratories) for 10 min at RT, washed three times 5 min in PBS, incubated
425 with secondary antibodies (Streptavidin-Alexa Fluor 405, Donkey anti-Chick Alexa Fluor
426 594, in M.O.M. Diluent) for 30 min at RT, washed three times 5 min in PBS. For
427 Pax7/Myod/Myog triple staining, sections were further blocked with anti-Pax7 antibody (in
428 M.O.M. Diluent) for 1 h at RT, washed three times 5 min in PBS, incubated with Alexa Fluor
429 488-conjugated anti-Myogenin and DyLight 550-conjugated anti-Myod antibodies (see
430 below, in M.O.M. Diluent) overnight at 4°C, washed in PBS three times 5 min and mounted
431 in PBS Glycerol 75%. EdU incorporation was detected with the Click-iT Plus Alexa Fluor
432 488 Imaging Kit (ThermoFisher) as recommended.

433 Immunostainings were analysed with a Zeiss Observer.Z1 and a Zeiss LSM800 confocal
434 microscopes. Images were processed with Imaris 7.2.1 software. For each cell pair, the
435 daughter cells were named 'Cell A' and 'Cell B'. Fluorescence intensity was measured on
436 segmented nuclei and expressed as a fraction of the maximum intensity between Cell A and
437 Cell B. In case of absence of signal in both daughter cells (*eg.* symmetric absence of Pax7),
438 the normalized fluorescence intensity was not determined (nd value).

439

440 Antibody fluorescent labeling

441 Anti-myogenin antibody (5FD, DSHB) was purified with protein G sepharose (Sigma)
442 as recommended. Briefly, hybridoma supernatant was incubated with protein G sepharose
443 overnight at 4°C and packed into polypropylene columns (Qiagen), washed five times with
444 PBS and antibody was eluted twice with 1.5 ml glycine 100 mM pH 2.7, neutralized with 150
445 μ l Tris 1M pH 9. Elution fractions were pooled and dialyzed (ThermoFisher) against PBS
446 overnight at 4°C. Antibody was concentrated with Amicon Ultra centrifugal filters (Merck) to
447 1 mg/ml. 100 μ l of purified F5D antibody at 1 mg/ml (resp. anti-Myod at 0.75 mg/ml (BD
448 Bioscience)) were dialysed (Thermofisher) against NaHCO₃ 100 mM pH 8.3 (resp. Na₂B₄O₇
449 50 mM pH 8.5) overnight at 4°C, incubated with 120 μ M Alexa Fluor 488 NHS ester
450 (ThermoFisher)(resp. 60 μ M DyLight 405 NHS ester (ThermoFisher) or 70 μ M DyLight 550
451 NHS ester (ThermoFisher)) at 23°C for 1 h. NaCl concentration was adjusted to 150 mM and
452 excess fluorescent dye was removed with Pierce Dye Removal Columns (ThermoFisher)
453 following manufacturer's recommendations. Desalted labeled antibodies were further
454 dialysed (ThermoFisher, Cat#69570) against PBS overnight at 4°C and stored at -20°C with 1
455 mg/ml bovine serum albumin (Sigma) and 50% glycerol.

456

457

458 **Data availability**

459 All data supporting the findings of this study are available from the corresponding author on
460 reasonable request.

461

462 **References**

- 463 1. Xu, M. *et al.* Partitioning of histone H3-H4 tetramers during DNA replication-
464 dependent chromatin assembly. *Science* **328**, 94–8 (2010).
- 465 2. Ahmad, K. & Henikoff, S. The histone variant H3.3 marks active chromatin by
466 replication-independent nucleosome assembly. *Mol. Cell* **9**, 1191–200 (2002).
- 467 3. Tran, V., Lim, C., Xie, J. & Chen, X. Asymmetric division of *Drosophila* male
468 germline stem cell shows asymmetric histone distribution. *Science* **338**, 679–682
469 (2012).
- 470 4. Kimura, H. & Cook, P. R. Kinetics of core histones in living human cells: little
471 exchange of H3 and H4 and some rapid exchange of H2B. *J. Cell Biol.* **153**, 1341–53
472 (2001).
- 473 5. Dion, M. F. *et al.* Dynamics of Replication-Independent Histone Turnover in Budding
474 Yeast. *Science (80-.)*. **315**, 1405–1408 (2007).
- 475 6. Verzijlbergen, K. F. *et al.* Recombination-induced tag exchange to track old and new
476 proteins. *Proc. Natl. Acad. Sci. U. S. A.* **107**, 64–8 (2010).
- 477 7. Deal, R. B., Henikoff, J. G. & Henikoff, S. Genome-Wide Kinetics of Nucleosome
478 Turnover Determined by Metabolic Labeling of Histones. *Science (80-.)*. **328**, 1161–
479 1164 (2010).
- 480 8. Filipescu, D., Müller, S. & Almouzni, G. Histone H3 Variants and Their Chaperones
481 During Development and Disease: Contributing to Epigenetic Control. *Annu. Rev. Cell*
482 *Dev. Biol.* **30**, 615–646 (2014).
- 483 9. Yadav, T., Quivy, J.-P. & Almouzni, G. Chromatin plasticity: A versatile landscape
484 that underlies cell fate and identity. *Science (80-.)*. **361**, 1332–1336 (2018).
- 485 10. Keppler, A. *et al.* A general method for the covalent labeling of fusion proteins with
486 small molecules in vivo. *Nat. Biotechnol.* **21**, 86–89 (2003).
- 487 11. Hinner, M. J. & Johnsson, K. How to obtain labeled proteins and what to do with them.
488 *Curr. Opin. Biotechnol.* **21**, 766–776 (2010).
- 489 12. Yang, G. *et al.* Genetic targeting of chemical indicators in vivo. *Nat. Methods* **12**, 137–
490 139 (2014).
- 491 13. Kohl, J. *et al.* Ultrafast tissue staining with chemical tags. *Proc. Natl. Acad. Sci. U. S.*

- 492 A. **111**, E3805-14 (2014).
- 493 14. Keppler, A. *et al.* Labeling of fusion proteins of O6-alkylguanine-DNA
494 alkyltransferase with small molecules in vivo and in vitro. *Methods* **32**, 437–444
495 (2004).
- 496 15. Bodor, D. L., Valente, L. P., Mata, J. F., Black, B. E. & Jansen, L. E. T. Assembly in
497 G1 phase and long-term stability are unique intrinsic features of CENP-A
498 nucleosomes. *Mol. Biol. Cell* **24**, 923–32 (2013).
- 499 16. Ray-Gallet, D. *et al.* Dynamics of histone H3 deposition in vivo reveal a nucleosome
500 gap-filling mechanism for H3.3 to maintain chromatin integrity. *Mol. Cell* **44**, 928–941
501 (2011).
- 502 17. Adam, S., Polo, S. E. & Almouzni, G. Transcription recovery after DNA damage
503 requires chromatin priming by the H3.3 histone chaperone HIRA. *Cell* **155**, 94–106
504 (2013).
- 505 18. Clément, C. *et al.* High-resolution visualization of H3 variants during replication
506 reveals their controlled recycling. *Nat. Commun.* **9**, 3181 (2018).
- 507 19. Deaton, A. M. *et al.* Enhancer regions show high histone H3.3 turnover that changes
508 during differentiation. *Elife* **5**, (2016).
- 509 20. Morrison, S. J. & Kimble, J. Asymmetric and symmetric stem-cell divisions in
510 development and cancer. *Nature* **441**, 1068–1074 (2006).
- 511 21. Knoblich, J. A. Mechanisms of asymmetric stem cell division. *Cell* **132**, 583–597
512 (2008).
- 513 22. Tajbakhsh, S. & Gonzalez, C. Biased segregation of DNA and centrosomes: moving
514 together or drifting apart? *Nat. Rev. Mol. Cell Biol.* **10**, 804–810 (2009).
- 515 23. Nakano, S., Stillman, B. & Horvitz, H. R. Replication-coupled chromatin assembly
516 generates a neuronal bilateral asymmetry in *C. elegans*. *Cell* **147**, 1525–36 (2011).
- 517 24. Xie, J. *et al.* Histone H3 threonine phosphorylation regulates asymmetric histone
518 inheritance in the *Drosophila* male germline. *Cell* **163**, 1–14 (2015).
- 519 25. Reznik, M. Thymidine-3H uptake by satellite cells of regenerating skeletal muscle. *J.*
520 *Cell Biol.* **40**, 568–571 (1969).
- 521 26. Gayraud-Morel, B., Chrétien, F. & Tajbakhsh, S. Skeletal muscle as a paradigm for
522 regenerative biology and medicine. *Regen. Med.* **4**, 293–319 (2009).
- 523 27. Kuang, S., Kuroda, K., Le Grand, F. & Rudnicki, M. A. Asymmetric self-renewal and
524 commitment of satellite stem cells in muscle. *Cell* **129**, 999–1010 (2007).
- 525 28. Rocheteau, P., Gayraud-Morel, B., Siegl-Cachedenier, I., Blasco, M. A. & Tajbakhsh,

- 526 S. A subpopulation of adult skeletal muscle stem cells retains all template DNA strands
527 after cell division. *Cell* **148**, 112–125 (2012).
- 528 29. Yennek, S., Burute, M., Théry, M. & Tajbakhsh, S. Cell adhesion geometry regulates
529 non-random DNA segregation and asymmetric cell fates in mouse skeletal muscle stem
530 cells. *Cell Rep.* **7**, 961–970 (2014).
- 531 30. Lukjanenko, L. *et al.* Loss of fibronectin from the aged stem cell niche affects the
532 regenerative capacity of skeletal muscle in mice. *Nat. Med.* **22**, 897–905 (2016).
- 533 31. Dumont, N. A. *et al.* Dystrophin expression in muscle stem cells regulates their
534 polarity and asymmetric division. *Nat. Med.* **21**, 1455–1463 (2015).
- 535 32. Sambasivan, R. *et al.* Distinct regulatory cascades govern extraocular and pharyngeal
536 arch muscle progenitor cell fates. *Dev. Cell* **16**, 810–821 (2009).
- 537 33. Théry, M. *et al.* The extracellular matrix guides the orientation of the cell division axis.
538 *Nat. Cell Biol.* **7**, 947–953 (2005).
- 539 34. Freida, D. *et al.* Human bone marrow mesenchymal stem cells regulate biased DNA
540 segregation in response to cell adhesion asymmetry. *Cell Rep.* **5**, 601–610 (2013).
- 541 35. Dumont, N. A., Wang, Y. X. & Rudnicki, M. A. Intrinsic and extrinsic mechanisms
542 regulating satellite cell function. *Development* **142**, 1572–1581 (2015).
- 543 36. Voog, J. & Jones, D. L. Stem cells and the niche: a dynamic duo. *Cell Stem Cell* **6**,
544 103–115 (2010).
- 545 37. Bentzinger, C. F., Wang, Y. X., Dumont, N. A. & Rudnicki, M. A. Cellular dynamics
546 in the muscle satellite cell niche. *EMBO Rep.* **14**, 1062–1072 (2013).
- 547 38. Kim, Y. H. *et al.* Cell cycle-dependent differentiation dynamics balances growth and
548 endocrine differentiation in the pancreas. *PLoS Biol.* **13**, 1–25 (2015).
- 549 39. Yu, C. *et al.* A mechanism for preventing asymmetric histone segregation onto
550 replicating DNA strands. *Science (80-.)*. **361**, 1386–1389 (2018).
- 551 40. Petryk, N. *et al.* MCM2 promotes symmetric inheritance of modified histones during
552 DNA replication. *Science (80-.)*. **361**, 1389–1392 (2018).
- 553 41. Wooten, M. *et al.* Asymmetric Histone Incorporation During DNA Replication in
554 *Drosophila* Male Germline Stem Cells. *bioRxiv* doi: <https://doi.org/10.1101/242768>
555 (2018). doi:10.2139/ssrn.3155700
- 556 42. Lansdorp, P. M. Immortal strands? Give me a break. *Cell* **129**, 1244–1247 (2007).
- 557 43. García del Arco, A., Edgar, B. A. & Erhardt, S. In vivo analysis of centromeric
558 proteins reveals a stem cell-specific asymmetry and an essential role in differentiated,
559 non-proliferating cells. *Cell Rep.* **22**, 2094–2106 (2018).

- 560 44. Siwek, W., Gómez-Rodríguez, M., Sobral, D., Jr, I. R. C. & Jansen, L. E. T. time-
561 ChIP: A Method to Determine Long-Term Locus- Specific Nucleosome Inheritance.
562 *Methods Mol. Biol.* **1832**, (2018).
- 563 45. Mathew, S. J. *et al.* Connective tissue fibroblasts and Tcf4 regulate myogenesis.
564 *Development* **138**, 371–384 (2011).
- 565 46. Muzumdar, M. D., Tasic, B., Miyamichi, K., Li, L. & Luo, L. A global double-
566 fluorescent Cre reporter mouse. *Genesis* **45**, 593–605 (2007).
- 567 47. Livak, K. J. & Schmittgen, T. D. Analysis of relative gene expression data using real-
568 time quantitative PCR and the $2^{-\Delta\Delta CT}$ method. *Methods* **25**, 402–408 (2001).
- 569 48. Rumbaugh, G. & Miller, C. A. Epigenetic changes in the brain: measuring global
570 histone modifications. *Methods Mol. Biol.* **670**, 263–274 (2010).
- 571 49. Gayraud-Morel, B. *et al.* A role for the myogenic determination gene Myf5 in adult
572 regenerative myogenesis. *Dev. Biol.* **312**, 13–28 (2007).
- 573 50. Tinevez, J.-Y. *et al.* TrackMate: An open and extensible platform for single-particle
574 tracking. *Methods* **115**, 80–90 (2017).
- 575 51. Vignaud, T., Ennomani, H. & Théry, M. Polyacrylamide hydrogel micropatterning.
576 *Methods Cell Biol.* **120**, 93–116 (2014).
- 577 52. Urciuolo, A. *et al.* Collagen VI regulates satellite cell self-renewal and muscle
578 regeneration. *Nat. Commun.* **4**, 1–26 (2013).

579

580 **Acknowledgments**

581 This work was supported by Institut Pasteur and grants from Agence Nationale de la
582 Recherche (Laboratoire d'Excellence Revive, Investissement d'Avenir; ANR-10-LABX-73,
583 ANR-16-CE12-0024) and Association Française contre les Myopathies, CNRS, and the
584 European Research Council (Advanced Research Grant 332893). We would like to thank the
585 Mouse Genetics Engineering Platform (Institut Pasteur), the Flow Cytometry and Photonic
586 Bioimaging Platforms of the Center for Technological Resources and Research (Institut
587 Pasteur), Johan van der Vlag (Radboud University, Netherlands) for providing the H3.1
588 antibody, Glenda Comai (Institut Pasteur) for initial assistance with confocal imaging, Dan
589 Filipescu for his advice to establish the mouse H3-SNAP variants, and Tom Cheung (Hong
590 Kong University of Science & Technology) for advice on antibody labeling. G.A. received
591 support from ANR.

592

593

594 **Author contributions**

595 B.E. and S.T. proposed the concept, designed the experiments, and wrote the paper. B.E.
596 performed and analysed the experiments. G.L.C. provided technical support. G.A. contributed
597 to application for the project, advised on experiments and edited the paper. All authors read
598 and agreed on the manuscript.

599

600 **Competing interests**

601 The authors declare no competing interests.

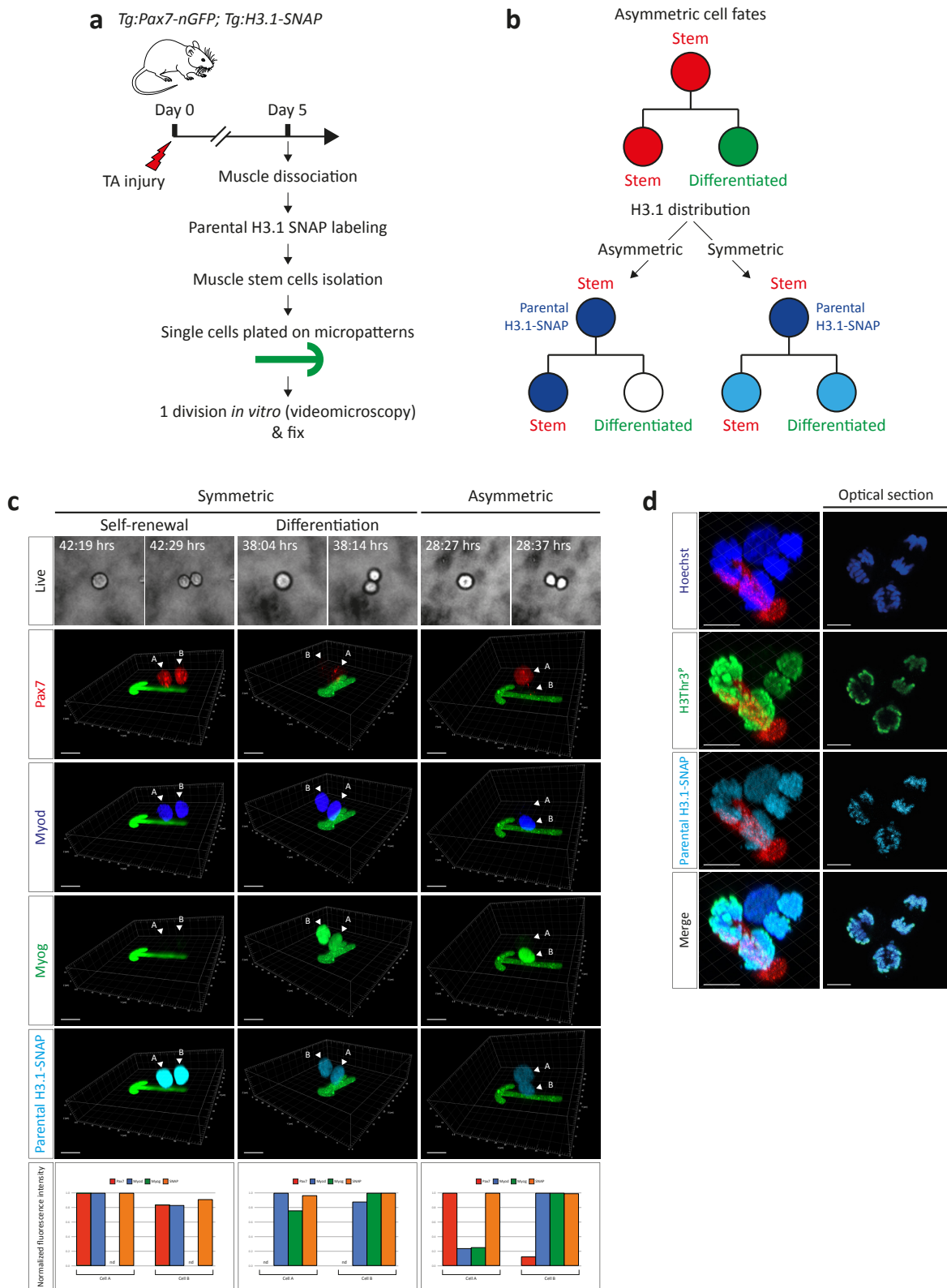
602

603 **Materials and correspondence**

604 Correspondence and material requests should be addressed to
605 shahragim.tajbakhsh@pasteur.fr

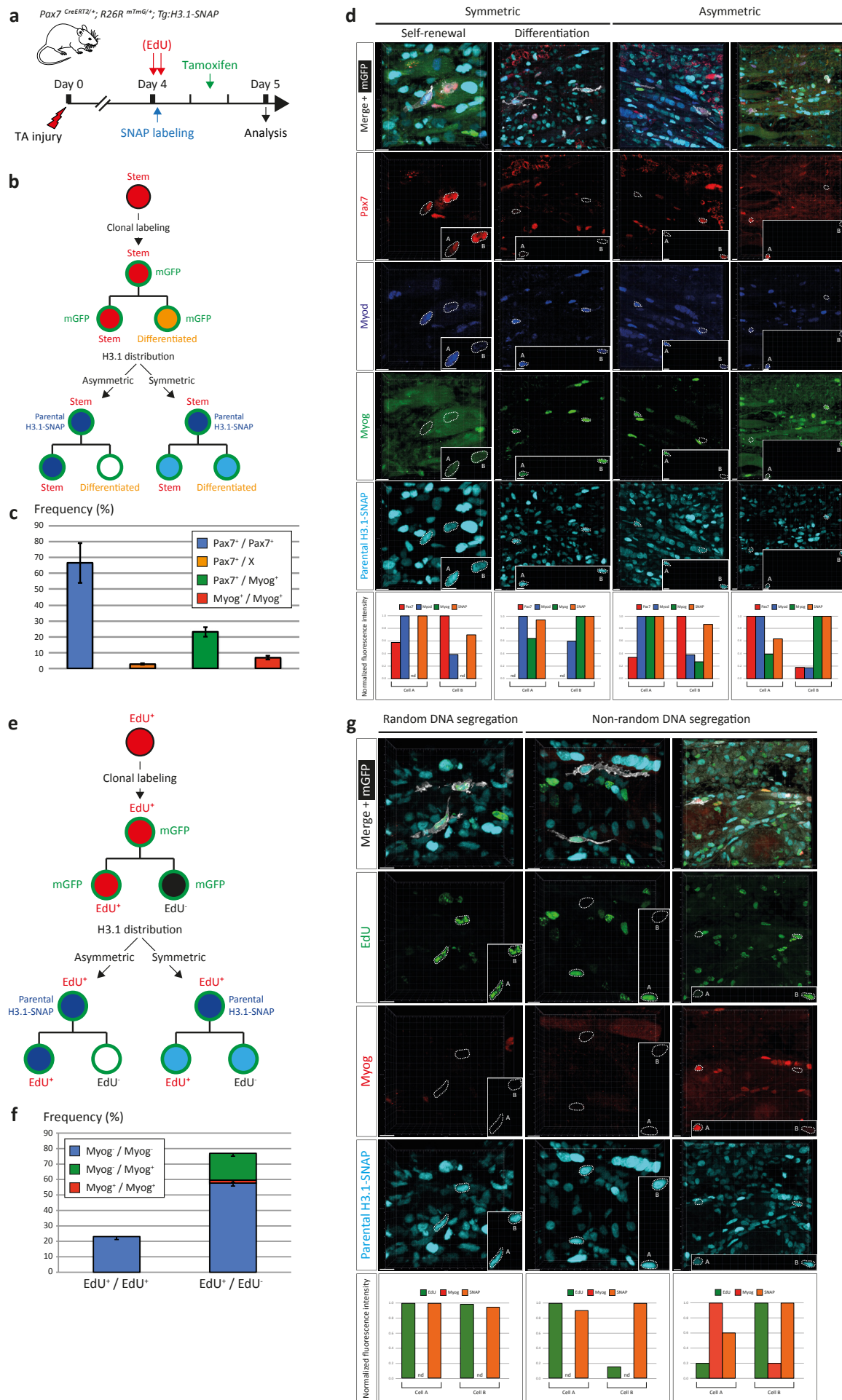
607

Fig. 1



609 **Fig. 1 Parental H3.1 histones are symmetrically distributed during asymmetric cell fate**
610 **decisions *ex vivo*.** **a**, Experimental scheme. **b**, Potential parental histone distribution patterns.
611 **c**, Representative examples of parental H3.1 inheritance pattern during SCD, towards self-
612 renewal (left) or differentiation (middle), or ACD (right). Arrowheads indicate nuclei of
613 daughter cells. For each cell pair, the daughter cells were named ‘Cell A’ and ‘Cell B’.
614 Fluorescence intensity was measured on segmented nuclei and expressed as a fraction of the
615 maximum intensity between Cell A and Cell B. In case of absence of signal in both daughter
616 cells (*eg.* symmetric absence of Pax7), the normalized fluorescence intensity was not
617 determined (nd value). n=4 mice, n=100 cell divisions/mouse. **d**, H3T3^P signal colocalizes
618 with H3.1-SNAP signal. n=3 mice. n=10 cell divisions/mouse. Scale bar 10 μ m.

Fig. 2



621

622 **Fig. 2 Parental H3.1 histones are symmetrically distributed during asymmetric cell fate**
623 **decisions and non-random DNA segregation *in vivo*.** **a**, Experimental scheme. Lineage-
624 tracing was tamoxifen-induced 14 h before analysis; parental histones were labeled 8 h before
625 tamoxifen administration; old DNA strands were labeled with EdU (Fig. 2e, 2f and 2g) 9 and
626 7 h before tamoxifen administration. **b**, Potential parental histone distribution patterns during
627 asymmetric cell fate decisions. **c**, Frequencies of the different modes of cell division. Rare
628 examples of Pax7/X and Myog/X daughter cells were observed, where one daughter cell
629 expresses Pax7 or Myog and the other neither Pax7 nor Myog. n=3 mice, n=147 divisions.
630 Data are presented as mean \pm SEM. **d**, Representative examples of parental H3.1 inheritance
631 pattern during SCD, towards self-renewal (left) or differentiation (middle-left), or ACD
632 (middle-right and right). The mGFP signal from labeled daughter cells is shown only in the
633 merged image for clarity; nuclei of daughter cells are outlined. Insets show nuclei of daughter
634 cells isolated from other cells. For each cell pair, the daughter cells were named 'Cell A' and
635 'Cell B'. Fluorescence intensity was measured on segmented nuclei and expressed as a
636 fraction of the maximum intensity between Cell A and Cell B. In case of absence of signal in
637 both daughter cells (*eg.* symmetric absence of Pax7), the normalized fluorescence intensity
638 was not determined (nd value). See Supplementary Fig. 2a for corresponding low
639 magnification images showing the clonality of the analysed events. Scale bar 10 μ m. **e**,
640 Potential parental histone distribution patterns during non-random DNA segregation. **f**,
641 Frequencies of the different modes of DNA segregation (random EdU⁺/EdU⁺ and non-random
642 EdU⁺/EdU⁻) and fate decisions assessed by Myogenin expression. n=2 mice, n=52 divisions.
643 Data are presented as mean \pm SEM. **g**, Representative examples of parental H3.1 inheritance
644 pattern during random DNA segregation (left) or non-random DNA segregation (middle and
645 right), with symmetric absence of Myogenin expression (left and middle) or asymmetric

646 Myogenin expression (right). The mGFP signal from labeled daughter cells is shown only in
647 the merged image for clarity; nuclei of daughter cells are outlined. Insets show nuclei of
648 daughter cells isolated from other cells. For each cell pair, the daughter cells were named
649 ‘Cell A’ and ‘Cell B’. Fluorescence intensity was measured on segmented nuclei and
650 expressed as a fraction of the maximum intensity between Cell A and Cell B. In case of
651 absence of signal in both daughter cells (*eg.* symmetric absence of Myog), the normalized
652 fluorescence intensity was not determined (nd value). See Supplementary Fig. 2c for
653 corresponding low magnification images showing the clonality of the analysed events. Scale
654 bar 10 μm .

655

656 **Statistical information**

657 Bar charts represent the mean \pm standard error of the mean (SEM) or standard deviation of the
658 mean (SD) as specified.

659

660 **Supplementary information**

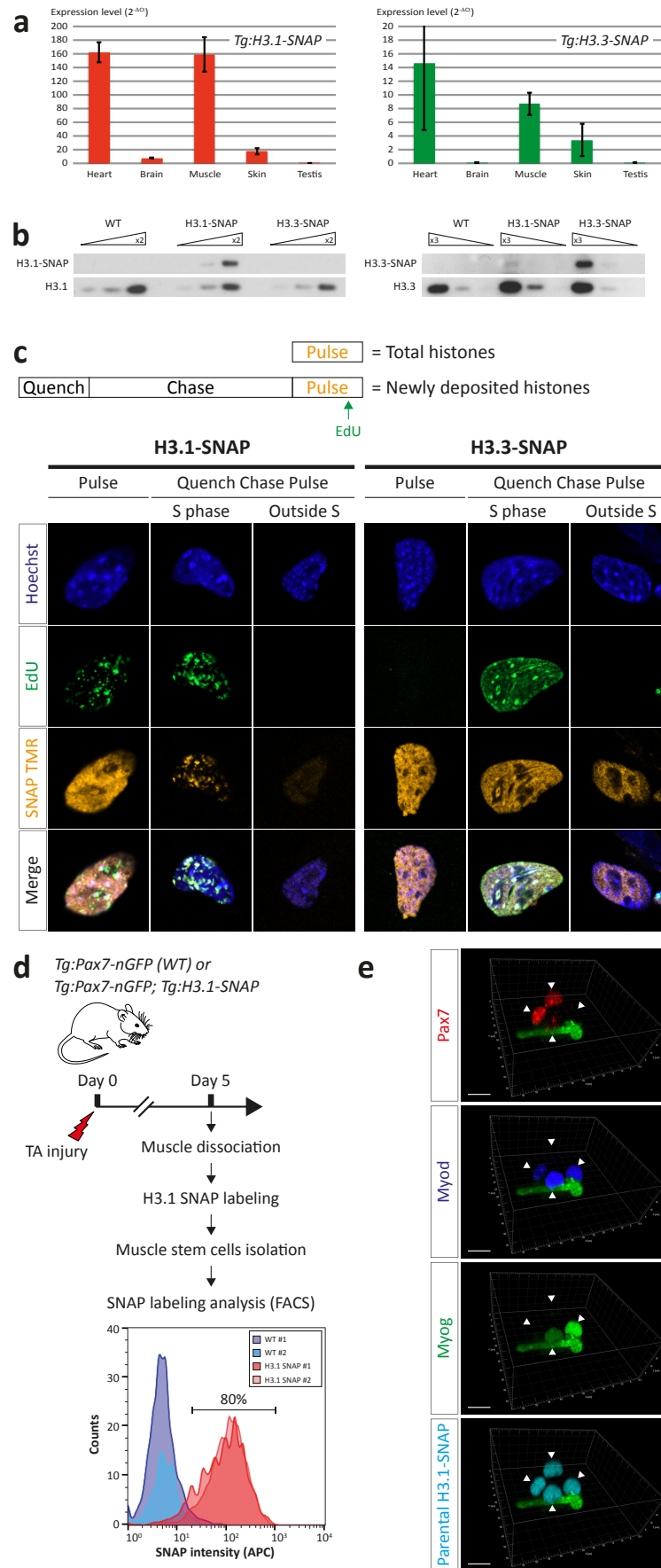
661

662 **Supplementary figures**

664

665

Supplementary Fig. 1

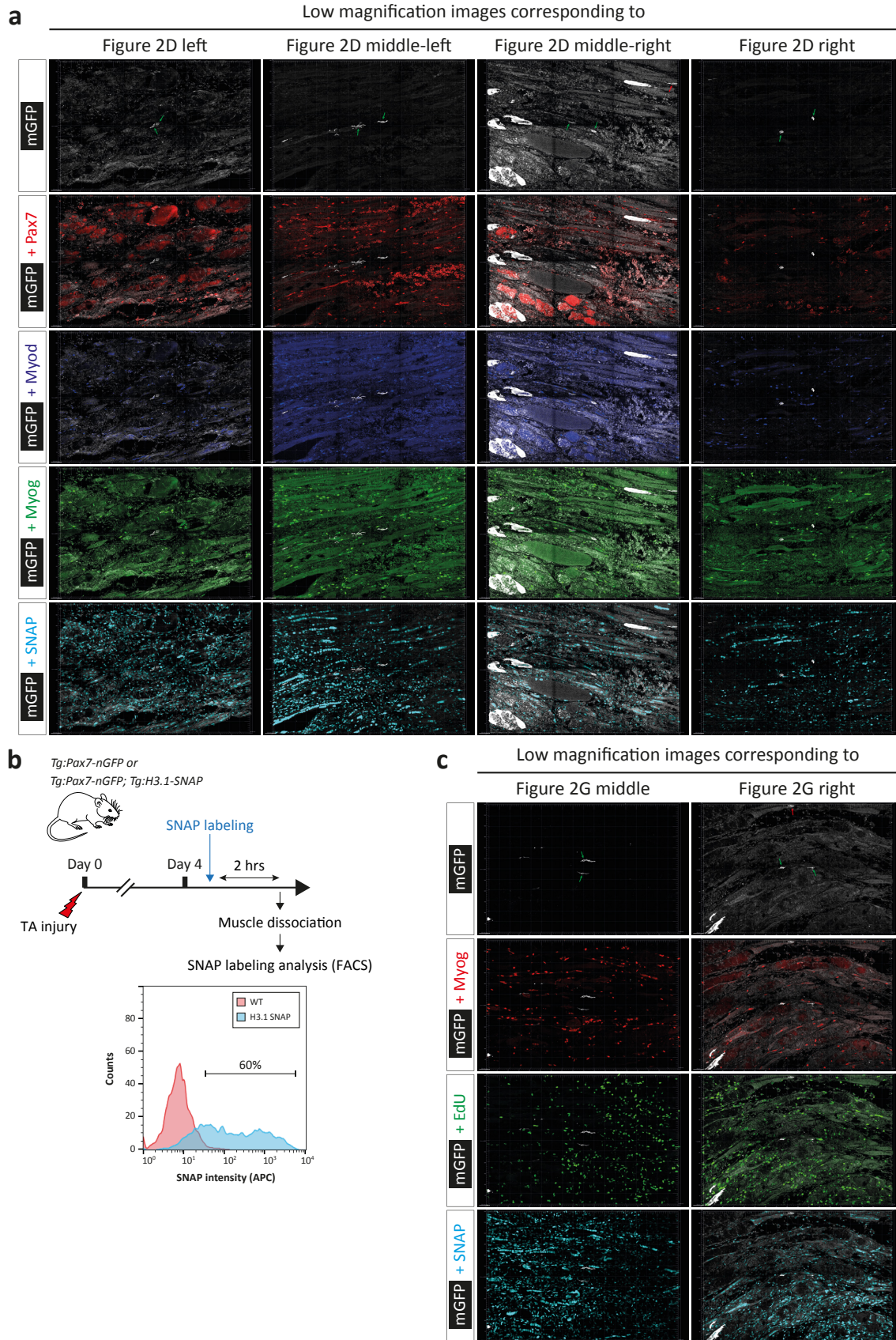


668 **Supplementary Fig. 1 *Tg:H3.1-SNAP* and *Tg:H3.3-SNAP* reporter lines validation and**
669 ***ex vivo* SNAP labeling of satellite cells. a,** Transgene expression level (RT-qPCR) from
670 heart, brain, skeletal muscle, skin and testis; n=2 mice per genotype. Data are presented as
671 mean \pm SD. **b,** Transgene expression level (Western blot) from primary embryonic fibroblasts
672 derived from WT, *Tg:H3.1-SNAP* and *Tg:H3.3-SNAP* mice, detected with anti-H3.1 (left) or
673 anti-H3.3 (right) antibodies. Each panel shows the endogenous (bottom) and SNAP-tagged
674 (top) histone variant. Triangles indicate different amounts of material loaded, centered on 1
675 μ g. **c,** SNAP TMR labeling of total (Pulse) or newly deposited (Quench Chase Pulse) SNAP-
676 tagged histone variants and DNA replication sites (EdU) in *Tg:H3.1-SNAP* and *Tg:H3.3-*
677 *SNAP* primary fibroblasts as in¹⁶. **d,** Efficiency of *ex vivo* SNAP labeling of satellite cells.
678 80% of *Tg:H3.1-SNAP* satellite cells were labeled compared to WT control cells; n=2 mice
679 per genotype. **e,** Example of a four-cell clone with two Pax7+ cells and two Myog+ cells on a
680 micropattern. Myog+ differentiated cells have left the cell cycle, therefore the 4-cell clone can
681 result from an ACD where the Pax7+ daughter undergoes a SCD, then ACD; another
682 possibility is an initial SCD, then each daughter undergoes an ACD. No cell death was
683 observed. Scale bar 10 μ m.

685

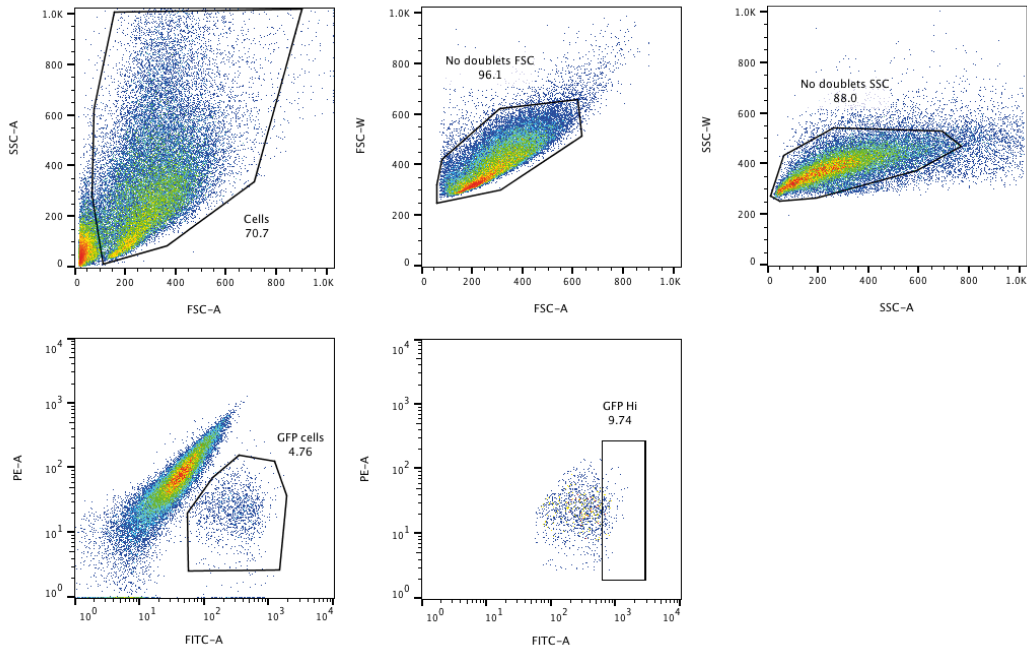
686

Supplementary Fig. 2



689 **Supplementary Fig. 2 *In vivo* SNAP labeling of satellite cells and clonality of the**
690 **analysed *in vivo* cell divisions. a,** Low magnification images (600 μm x 900 μm)
691 corresponding to high magnification images of Fig. 2d. Green arrows indicate mGFP-labeled
692 daughter cells; red arrows indicate presumably unrelated mGFP-labeled cells. Scale bar 50
693 μm . **b,** Efficiency of *in vivo* SNAP labeling of satellite cells at 4 dpi. 60% of *Tg:H3.1-SNAP*
694 satellite cells were labeled compared to WT control cells; n=2 mice per genotype. **c,** Low
695 magnification images (600 μm x 900 μm) corresponding to high magnification images of Fig.
696 2g. Green arrows indicate mGFP-labeled daughter cells; red arrows indicate presumably
697 unrelated mGFP-labeled cells. Scale bar 50 μm .

Supplementary Fig. 3



698

699 **Supplementary Fig. 3 Isolation of satellite cells by FACS.**

700 Satellite cells were isolated by FACS by gating first on size and granularity ('Cells' gate),
701 excluding doublets ('No doublets FSC' then 'No doublets SSC' gates) and gating on the
702 GFP+ population ('GFP cells' gate). Pax7-nGFP^{Hi} cells (top 10% highest nGFP-expressing
703 cells, 'GFP Hi' gate) were sorted.

704

Supplementary Table 1. Oligonucleotides used in this study

Oligonucleotide	Sequence
NotI_mH3.1_F	atgcgagcggccgcCGCCACCatggctcgtactaagcagaccgct
NotI_mH3.3_F	atgcgagcggccgcCGCCACCatggctcgtacaaagcagactgcc
DPPVAT_mH3.1_R	GGTGGCGACCGGTGGATCagcccgtcgcgggatacggcg
DPPVAT_mH3.3_R	GGTGGCGACCGGTGGATCagcacgttctccgcgtatcgggcg
DPPVAT_SNAP_F	GATCCACCGGTCGCCACCatggacaaagactgcgaa
BamHI_SNAP_R	Tttgatcctggcgcgcctatacctgc
CAG_For	GCAACGTGCTGGTTATTGTG
SV40 PolyA_F	CAATGTATCTTATCATGTCTGGATCGGG
SNAP qPCR_R	TCAGAATGGGCACGGGATTT
SNAP qPCR_F	CCAGCAGGAGAGCTTTACCC
CAG_R3	CATATATGGGCTATGAACTAATGACCCC
Tbp_F	ATCCCAAGCGATTTGCTG
Tbp_R	CCTGTGCACACCATTTTCC

705

706

Supplementary movies

708

Supplementary Movie 1.

710 Videomicroscopy of a Pax7-nGFP^{Hi} cell isolated from TA muscle at 5 dpi and plated on an
711 asymmetric micropattern (not visible), corresponding to Fig. 1c left. The movie was started
712 3 h after plating and continued for 40 h; images were taken every 9 min (bright-field, 10×
713 magnification).

714

Supplementary Movie 2.

716 Videomicroscopy of a Pax7-nGFP^{Hi} cell isolated from TA muscle at 5 dpi and plated on an
717 asymmetric micropattern (not visible), corresponding to Fig. 1c middle. The movie was
718 started 3 h after plating and continued for 40 h; images were taken every 9 min (bright-field,
719 10× magnification).

720

721 **Supplementary Movie 3.**

722 Videomicroscopy of a Pax7-nGFP^{Hi} cell isolated from TA muscle at 5 dpi and plated on an
723 asymmetric micropattern (not visible), corresponding to Fig. 1c right. The movie was started
724 3 h after plating and continued for 40 h; images were taken every 9 min (bright-field, 10×
725 magnification).